Title
Source location impact on relative tsunami strength along the U.S. West Coast

Authors
Rasmussen, L.
Bromirski, P. D
Miller, A. J
et al.

Data Availability
The data associated with this publication are available upon request.

Peer reviewed

Source location impact on relative tsunami strength along the U.S. West Coast

L. Rasmussen[1], P. D. Bromirski[1], A. J. Miller[1], D. Arcas[2,3], R. E. Flick[4], and M. C. Hendershott[1]

[1]Scripps Institution of Oceanography, University of California San Diego, La Jolla, California, USA, [2]NOAA Center for Tsunami Research, Pacific Marine Environmental Laboratory, National Oceanic and Atmospheric Administration, Seattle, Washington, USA, [3]Joint Institute for the Study of the Atmosphere and Ocean, University of Washington, Seattle, Washington, USA, [4]California Department of Parks and Recreation, Division of Boating and Waterways, Scripps Institution of Oceanography, La Jolla, California, USA

Abstract Tsunami propagation simulations are used to identify which tsunami source locations would produce the highest amplitude waves on approach to key population centers along the U.S. West Coast. The reasons for preferential influence of certain remote excitation sites are explored by examining model time sequences of tsunami wave patterns emanating from the source. Distant bathymetric features in the West and Central Pacific can redirect tsunami energy into narrow paths with anomalously large wave height that have disproportionate impact on small areas of coastline. The source region generating the waves can be as little as 100 km along a subduction zone, resulting in distinct source-target pairs with sharply amplified wave energy at the target. Tsunami spectral ratios examined for transects near the source, after crossing the West Pacific, and on approach to the coast illustrate how prominent bathymetric features alter wave spectral distributions, and relate to both the timing and magnitude of waves approaching shore. To contextualize the potential impact of tsunamis from high-amplitude source-target pairs, the source characteristics of major historical earthquakes and tsunamis in 1960, 1964, and 2011 are used to generate comparable events originating at the highest-amplitude source locations for each coastal target. This creates a type of "worst-case scenario," a replicate of each region's historically largest earthquake positioned at the fault segment that would produce the most incoming tsunami energy at each target port. An amplification factor provides a measure of how the incoming wave height from the worst-case source compares to the historical event.

1. Introduction

Tsunamis along the U.S. West Coast can cause significant damage to property in harbors and low-lying coastal zones. The relative magnitude and location of the largest amplitude waves along the West Coast varies considerably for different events, with some sites experiencing what appear to be either disproportionately large or small impacts. Some coastal impact is related to the local coastal morphology, nearby bathymetry, and wave orientation [*Keulegan et al.*, 1969; *Murty*, 1977]. Under some circumstances wave amplification may occur in bays, harbors, or along irregular coastlines due to internal resonance [*Horrillo et al.*, 2008; *Fuller and Mysak*, 1977; *Roberts and Kauper*, 1964]. The offshore magnitude of approaching wave trains can also vary by up to an order of magnitude over as little as 100–200 km of coastline [e.g., *Kowalik et al.*, 2008].

Tsunamis have very long wavelengths (with associated low wave number) that reach lengths of 50–200 km or more, depending on wave period. The pressure from gravity waves decays exponentially with depth as e^{-kz}, where z is depth and k the wave number. Thus, unlike ocean swell, very long period, very low wave number tsunamis feel the ocean bottom even in deep water (where their wavelength $>>$ ocean depth), and thus are strongly affected by irregular bottom topography. The interaction of tsunamis with the ocean bottom accordingly results in complicated peak wave amplitude patterns.

Factors affecting the maximum tsunami wave height at the shore include (1) the target's proximity to the source, (2) the orientation or azimuth of the source with respect to the target coastline, (3) scattering by local or remote bathymetry, and (4) amplification along the tsunami path caused by bathymetric reflection,

refraction, or scattering. A target's proximity to tsunami sources and its coastline exposure are primary factors in its vulnerability to the most destructive events, and these are usually straightforward to assess. Locally, coastline features may either amplify or disperse wave energy on arrival, through bay or harbor oscillations, focusing around headlands, or nearby obstacles such as small islands, submerged banks, and submarine canyons, as in the Southern California Bight.

However, the perturbation of passing tsunamis by variations in bathymetry can also have a persistent effect as propagation continues thousands of kilometers across the ocean [*Mofjeld et al.*, 2001; *Satake*, 1988; *Uslu et al.*, 2010]. Complex patterns of interference, scattering, and amplification may result, particularly when there is superposition of the original tsunami source with multiple effective secondary sources resulting from bathymetric irregularities [*Barberopoulou et al.*, 2014]. As a result, the amplitude and timing of the peak wave height at a specific target may be quite different for tsunami sources separated by relatively short distances, and proximate coastal targets may experience large differences in wave height from the same source. Consequently, wave height and potential impact can be difficult to predict [*Kowalik et al.*, 2008]. In addition, because the horizontal gradient of depth variations (feature width relative to height) can significantly affect wave amplitude, either increasing or decreasing, the resolution of model domains can also reduce the accuracy of predictions [*Kowalik et al.*, 2008; *Mofjeld et al.*, 2001].

Simulated tsunami propagation fields for source regions worldwide are part of a National Oceanic and Atmospheric Administration (NOAA) Center for Tsunami Research (NCTR) database. The NCTR model divides potential source regions—such as the extensive subduction zones surrounding much of the Pacific Rim—into 100 km × 50 km segments. Seafloor displacement is calculated for each segment based on local fault geometry and a standard slip magnitude; this provides the initial sea surface displacement in the tsunami propagation model. The set of source wave propagation time series then forms the building blocks for quickly simulating events by linear combination to generate deep water tsunami wave forecasts and warnings (in association with the DART buoy system). These can be used to produce tsunami hazard assessments of selected populated coastal areas as in the PMEL tsunami forecast series [*Tang et al.*, 2010; *Arcas and Uslu*, 2010], and for studying historical events. Because they are calculated from discrete, independent source segments, the time series of wavefields are uniquely suited for comparisons of tsunami propagation over variable distances, topography, and orientations.

Here we use the output of the NCTR propagation model for tsunamis generated by Pacific Rim seismic events to investigate the characteristics of source-target combinations that produce the highest amplitude waves with potential for the most damaging impact. We focus our analysis on six U.S. West Coast targets representing major population centers in Washington, Oregon, and California: the mouth of the Straight of Juan de Fuca, Washington (Seattle and Puget Sound communities); the mouth of the Columbia River at the Washington-Oregon border (Astoria, OR); Crescent City, CA, site of a frequently hard-hit harbor; San Francisco, Santa Monica Bay (Los Angeles), and San Diego, CA. Target coordinates were selected just offshore of each site near the shelfbreak, 30–40 km from shore at approximately 500 m depth, before the impact of small-scale shallow-water local topography and nonlinear effects require higher-resolution nested models to resolve nearshore wave heights [e.g., *Tang et al.*, 2010].

Model wave propagation fields for equal-displacement Pacific tsunami sources are examined to (i) identify the highest amplitude tsunami source locations for each target, (ii) locate any source-target combinations with unusually large wave height at the target, and (iii) identify characteristics and possible causes of wave amplification between source-target pairs. Ratios of tsunami spectra from key points in their propagation across the Pacific illustrate how prominent bathymetric features affect wave energy properties. To provide context with respect to known events, we compare the potential magnitude of tsunamis from maximum-amplitude source locations with historical tsunamis from the same regions.

2. Propagation Model and Unit Source Database

This analysis makes use of tsunami propagation simulations from NCTR's Short-term Inundation Forecast for Tsunamis (SIFT) database [*Gica et al.*, 2008] for 366 source locations around the Pacific Rim (Figure 1). All fault zones are divided into equal segments or "unit sources" that are 100 km in length (along-fault) by 50 km in width (cross-fault). Depending on the width of the subduction zone, there are 2–5 rows of unit sources for each 100 km length of seafloor, extending perpendicular to the trench axis in the direction of
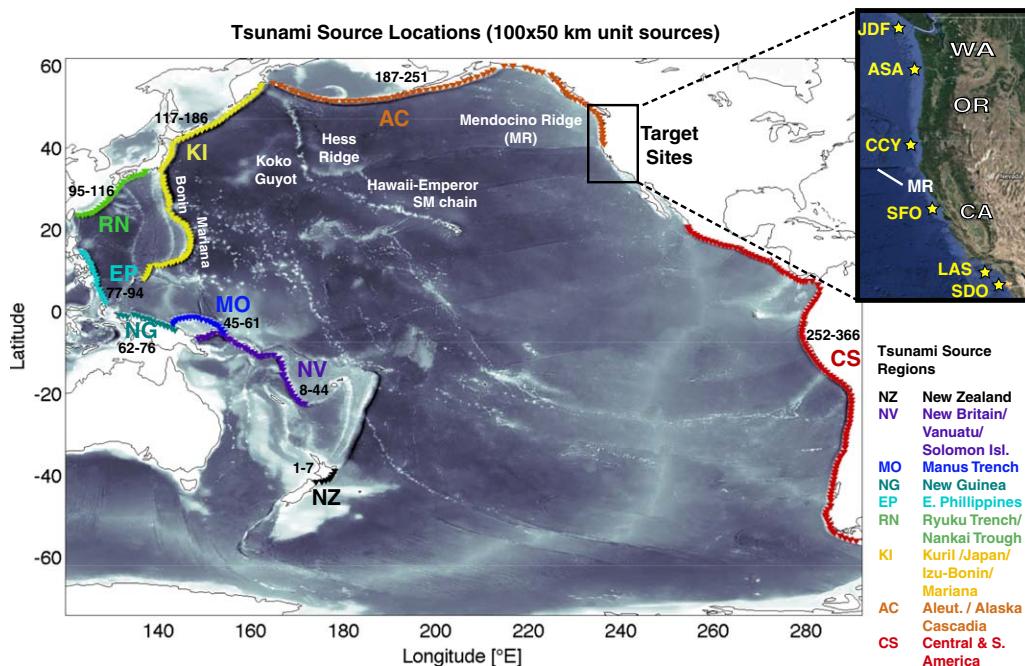
Figure 1. Locations of NCTR tsunami propagation model unit sources for the Pacific Rim and target sites near U.S. West Coast population centers. Each unit source is a 100 km × 50 km segment of a subduction zone capable of tsunami-generating earthquakes. Tsunami source regions are labeled with their NCTR identifier and color coded. Numbers along each segment (1–366) correspond to the clockwise order of sources used in the analysis.

slab subduction. Unit source depths depend on their cross-fault position in the subduction zone, but generally include a shallow source at approximately 5 km below the seafloor near the fault axis, and a deeper source around 10–20 km depth. Source dip and strike angles are specific to the local geology. For the purposes of our comparisons, the 10–20 km layer of unit sources (row A in the database) is used.

Propagation time series of wave height and velocity are computed for all unit sources using the Method of Splitting Tsunamis (MOST) model. MOST includes an elastic earthquake model to calculate the seafloor displacement according to the fault plane parameters for each source, and a standard 1 m slip is prescribed to simulate a Mw 7.5 event at all sites. The propagation model uses the nonlinear shallow-water wave equations in spherical coordinates solved numerically using a splitting method similar to that described by *Titov and González* [1997], with grid resolution adjusted to match physical dispersion as prescribed by linear theory. Because of the small amplitude of tsunamis in deep water (approximately 1 m over a wavelength of 100 km or more) and the low particle velocity compared to the wave velocity (1 versus 650 km h^{-1}), the deep water solution emerges as linear. As a result, the wave height and velocity calculated for individual unit sources can be combined linearly to simulate a tsunami generated by a larger fault area, and/or multiplied by an appropriate factor to replicate the actual slip magnitude that determines tsunami wave height [*Arcas and Segur*, 2012].

Tsunamis are especially affected by seafloor topography when transitioning from the deep ocean across continental shelves to coasts. Wave height and degree of inundation at the immediate shoreline can also be strongly affected by the near-coastal seafloor bathymetry and the geometry of the coastline, bay or harbor, which require very high resolution (10–50 m) model domains [*Titov and González*, 1997]. The 4′ resolution bathymetric grid used to generate NCTR's propagation database can sufficiently resolve most coastline configurations and is optimal for adjusting numerical dispersion to physical dispersion, but this resolution does not adequately resolve smaller features, such as those that occur in the Southern California Bight. Accordingly, shoreline impacts in MOST are modeled with high-resolution nested domains. The relative impact of different source locations on tsunami height approaching the U.S. West Coast are determined by comparison of the characteristic maximum wave heights at coordinates near 500 m depth offshore at our six target sites, i.e., after the deep-to-intermediate-depth continental slope transition occurs, but prior to the
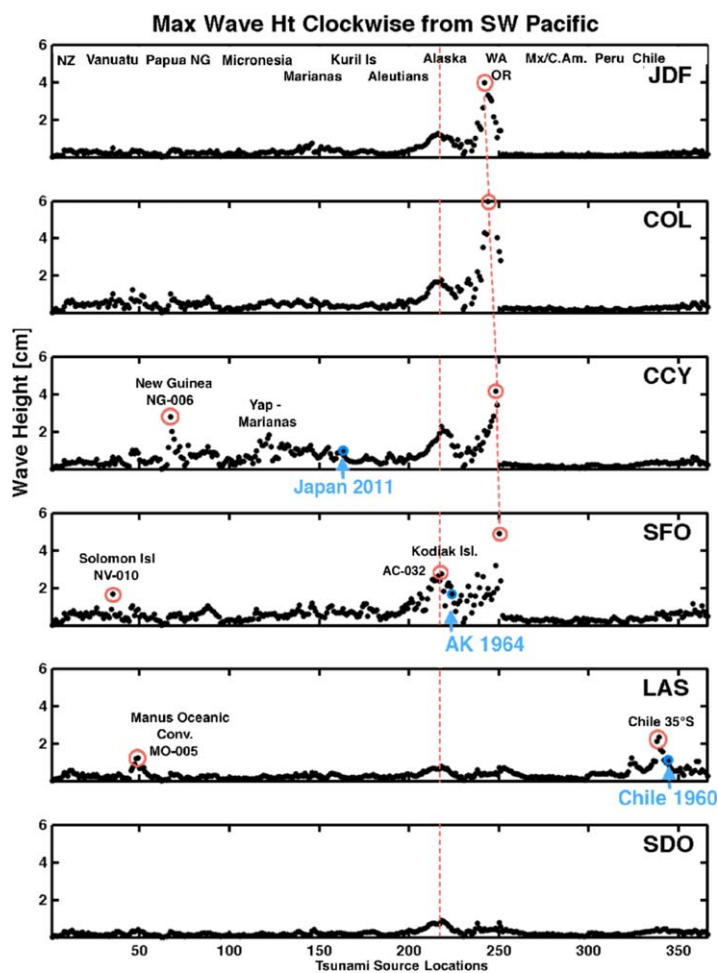
Figure 2. Peak wave height at six target sites from tsunami sources arranged clockwise around the Pacific. Numbering progresses from New Zealand (1–7) to SW Pacific (8–76), Philippines and far W Pacific (77–116), NW Pacific (117–186), Aleutians (187–211), Alaska-Canada (212–242), Washington-Oregon (243–251), Mexico-Central America (244–288), Colombia-Ecuador (289–305), Peru (306–323), and Chile (307–366). Tsunami generation is from the 10–20 km depth of each unit source (layer A), with base magnitude Mw 7.5, corresponding to a 1.0 m slip. Unit source fault length and width is 100 km × 50 km.

effect of shallow-water continental-shelf bathymetry dominating wave dynamics. Source coordinates and wave height data at the six target sites can be found in supporting information Table S1.

3. Wave Height Comparison by Source Location, Distance, and Direction

A direct comparison of maximum wave height for each unit source at the six target sites provides a straightforward overview of how wave height differs along the West Coast (Figure 2). Proceeding clockwise from the southwest Pacific (source 1 on *x* axis) to the southern tip of Chile (source 366), we see some patterns common between all targets, some common to only northern or southern targets, and some unique to only a single target. For example, all targets have elevated wave height from sources along approximately 1000 km of the Alaska coast, with the peak amplitude centered just south of Kodiak Island (Figure 2, vertical dotted line, and Figure 5, source AC-32). However, instead of decreasing with distance from the source, maximum wave height increases from Juan de Fuca to San Francisco, then abruptly decreases south of Point Conception, indicating that source distance is not the dominant factor and that distant or local topographic effects (such as island scattering, focusing by refraction, wave interference, or a combination of these) can play a significant role in tsunami amplitudes along the West Coast [e.g., *Satake*, 1988; *Rabinovich*, 1997; *Mofjeld et al.*, 2000; *Kowalik*, 2008]. In this case it is possible that waves propagating from north to south parallel to the coast are amplified by refractive coastal trapping [*Munk et al.*, 1956; *Rabinovich et al.*, 2006; *Mysak*, 1980]. In the lee south of Pt. Conception, where the coastline orientation shifts, the shelf broadens, and small islands and ridges populate the Southern California Bight, edge wave trapping processes would be interrupted. Shelf edge waves have also been explored as contributing factors to the unusual tsunami impact often observed at Crescent City, CA [*Gonzalez et al.*, 1995; *Horrillo et al.*, 2008; *Holmes-Dean et al.*, 2015].

The only instances in which wave height is clearly related to source distance occur where there are sources within 1000–1500 km of the target, such as the four northern sites which are in close proximity to the Alaskan/Cascadian subduction zones. At these locations, the nearest source causes the highest amplitude wave (Figure 2, dotted line with circled sources), and wave height decreases fairly steadily out to a distance of about 1000 km (Figure 3). From Juan de Fuca to the Columbia River, the nearest maximum source is located directly offshore in the Cascadia Subduction Zone (CSZ). In the San Francisco area, the nearest potential
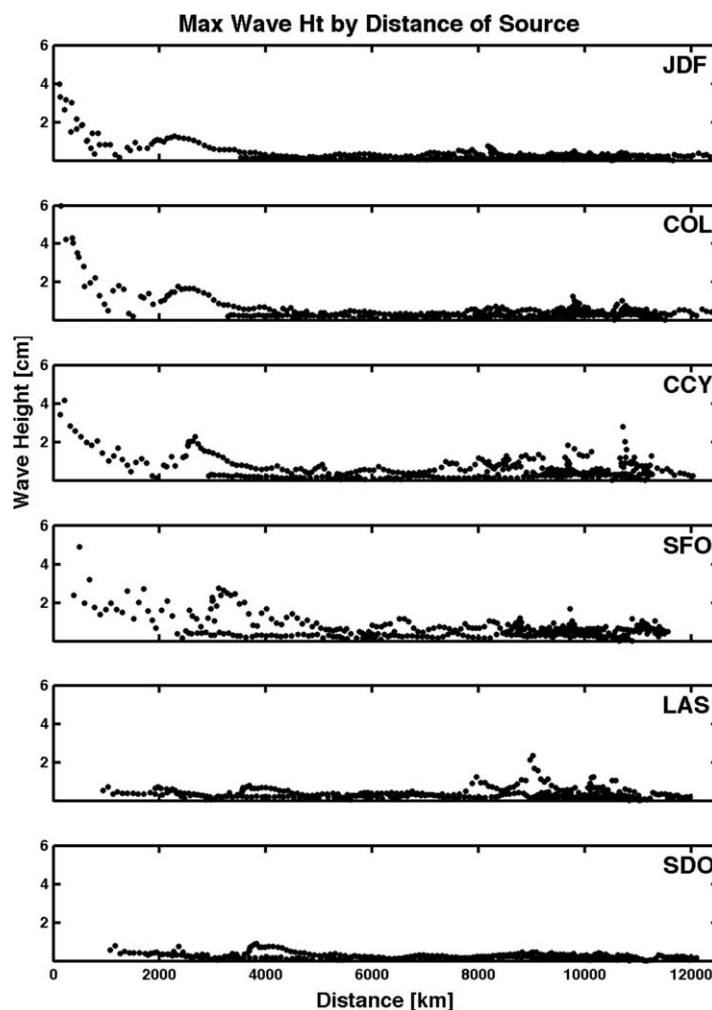
Figure 3. Peak wave height at six target sites sorted by source direction.

strong tsunami source region is at the southernmost extent of the CSZ, about 300 km to the north. For the southern California targets, CSZ sources do not produce significant tsunami amplitudes on approach to the continental shelf.

Elevated wave heights from southern Chile unit sources occur at all target sites, but decrease north of San Francisco. The highest amplitude waves in the Los Angeles area result from sources along a 3000 km zone along the South American coast centered near 35°S. The azimuth of Los Angeles area peak sources tend to cluster around 140° (Figure 4), a pattern quite different than that for targets to the north, which continue to increase in height as the azimuth approaches 150° (allowing waves to round Cape Mendocino). The more southerly orientation of the coastline near Los Angeles may also be a factor in the elevated wave heights there, as may remote bathymetric effects near the source or along the propagation path (see sections 4.1 and 5).

Elevated wave heights can result from small source areas affecting only one of the six target locations (e.g., northern New Guinea (NG) sources impact Crescent City, northern Solomon Islands (NV) sources impact only Los Angeles.) In some cases, just a single source location results in amplified wave heights at one target, such as source NV-010 in the Solomon Islands at San Francisco (Figure 5, and individual circled and labeled sources in Figure 2). In the following sections, we closely examine the wave propagation patterns associated with these remote source "outliers," and consider the effects of distant wave focusing, scattering, and interference as well as amplification by bathymetry nearer the target.

4. Tsunami Amplification by Remote Bathymetry

Tsunamis striking the U.S. West Coast can be influenced by numerous deep-ocean bathymetric features that produce diffraction and refraction patterns, resulting in both constructive and destructive interference and focusing and defocusing of wave energy. This is especially true for tsunamis that originate in the Western Pacific, which *Mofjeld et al.* [2001] refer to as a "scattering province," a region with a high density of bathymetric features smaller than a tsunami wavelength (approximately 400 km). Waves resulting from scattering by relatively small features can superimpose on broader-scale wave disturbances caused by larger bathymetric features, and are responsible for concentrations of wave energy resulting in the complex "fingers" of elevated maximum wave height that extend across the Pacific on maps of maximum tsunami height (e.g., Figure 6b). By contrast, "low scattering provinces" are defined as regions with few small
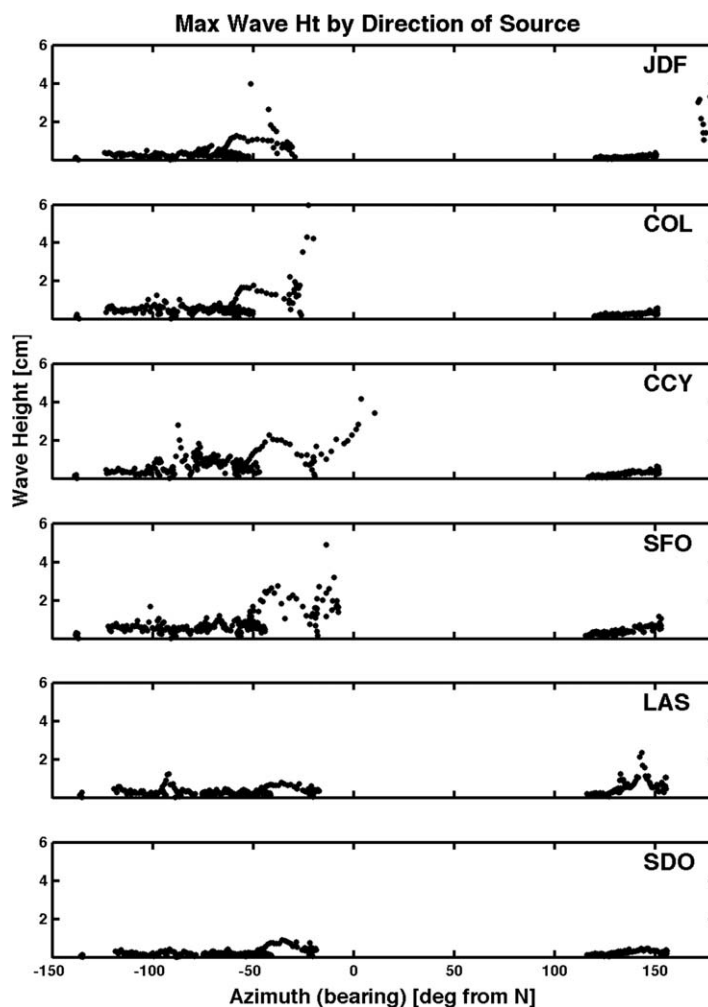
Figure 4. Peak wave height at six target sites sorted by source distance.

bathymetric features, which therefore cause little disturbance of the primary tsunami wave amplitude and propagation direction, e.g., the NE Pacific. The key feature in this region is the lengthy ridge along the Mendocino Fracture Zone, located at 40°N and extending about 2400 km from the California continental shelf westward into the central North Pacific. Depending on the orientation of the tsunami wavefronts with respect to the ridge axis, significant refraction and focusing of wave energy may occur as a tsunami passes over it. Maximum height maps show areas of focusing, but do not show how elevated wave heights evolved, or from which bathymetric features. Analysis of wave propagation (water height) time series, wave spectra, and/or wave velocity (to give local energy flux, e.g., *Satake* [1988]) discussed below illuminate the development of these high-energy paths.

4.1. West Pacific Tsunamis: Amplification Near the Source

Most of the significant increases in maximum wave amplitude observed as tsunamis cross the Pacific occur for waves that originate at particular source areas in the SW Pacific, the region with the highest "scattering index" [*Mofjeld et al.*, 2001]. Each of these source areas has a relatively small extent (100–200 km), resulting in a specific source-target pairing for which wave height is sharply elevated at different key West Coast locations: New Guinea-Crescent City (Figure 5, source NG-06), Solomon Islands-San Francisco (Figure 5, source NV-10), and Manus-Los Angeles (Figure 5, source NV-05). The largest West Coast wave height occurs for the New Guinea-Crescent City pairing, where there is a threefold increase in amplitude relative to waves from other nearby sources (Figure 2). Mapping maximum wave height taken from the propagation model for the peak source NG-06 (2.5°S, 139.6°E) reveals distinct high-amplitude bands across the Pacific (Figures 6b and 6c), starting with branches of very high energy (yellow) centered around the source. Moving away from the source location, a region of moderately high energy extends northwest towards Palau and southern Japan, broadly concentrated over the Kyushu-Palau Ridge in the central Philippine Sea, while the region of highest wave amplitude (Figure 6c, yellow region) extends northeast and separates into several branches. One of these branches is concentrated in a northward path over the West Marianas ridge and extends to central Japan. Another is located parallel to this over the Marianas Island chain, and veers northeast near the junction of the Mariana and Bonin ridge/trench system, eventually intersecting the Emperor Seamount chain. The third branch, which appears to be the most direct energy path from the tsunami source, extends through the Caroline Island cluster and northeastward directly toward Koko Guyot and Hess Rise (K and H in Figure 6b), two of the larger seafloor topographic features in the central North Pacific. These appear to scatter wave energy
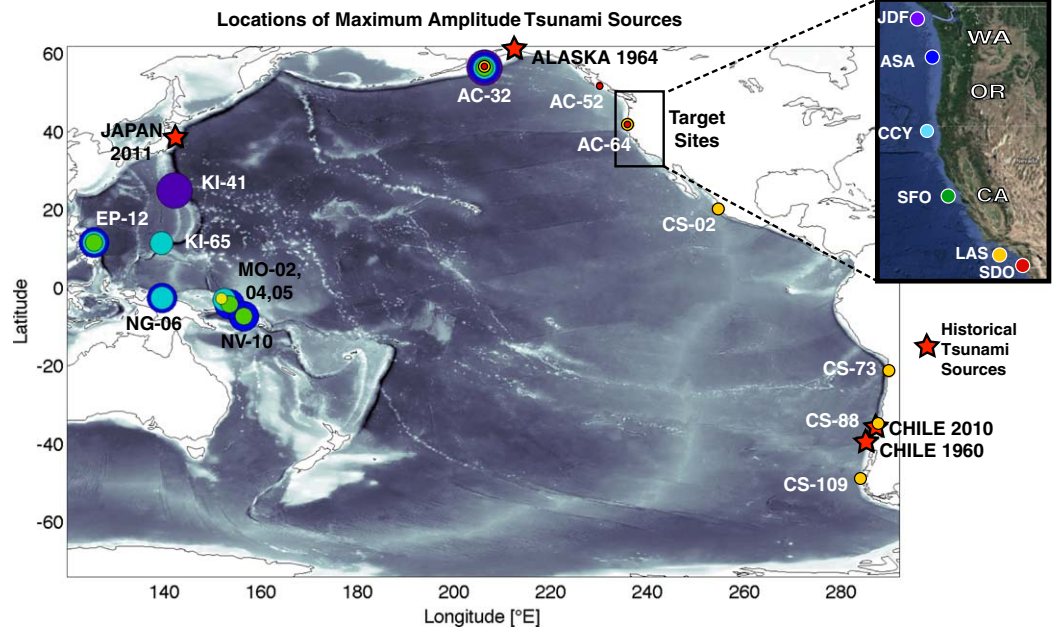
Figure 5. Unit source locations generating the largest amplitude waves at target sites on the U.S. West Coast. Sources are color coded for the affected target: Juan de Fuca (purple), Astoria, OR (blue), Crescent City (cyan), San Francisco (green), Los Angeles (yellow), and San Diego (red). Also shown are the locations of historic mega-earthquake tsunami sources: Chile 1960, Alaska 1964, Chile 2010, and Japan 2011 (red stars). Labels are the NCTR unit source ID.

propagating northward and serve as a waveguide to concentrate wave energy eastward directly toward the Mendocino Ridge (MR). While propagating over the ridge, a significant height increase develops that builds toward the Northern California coast.
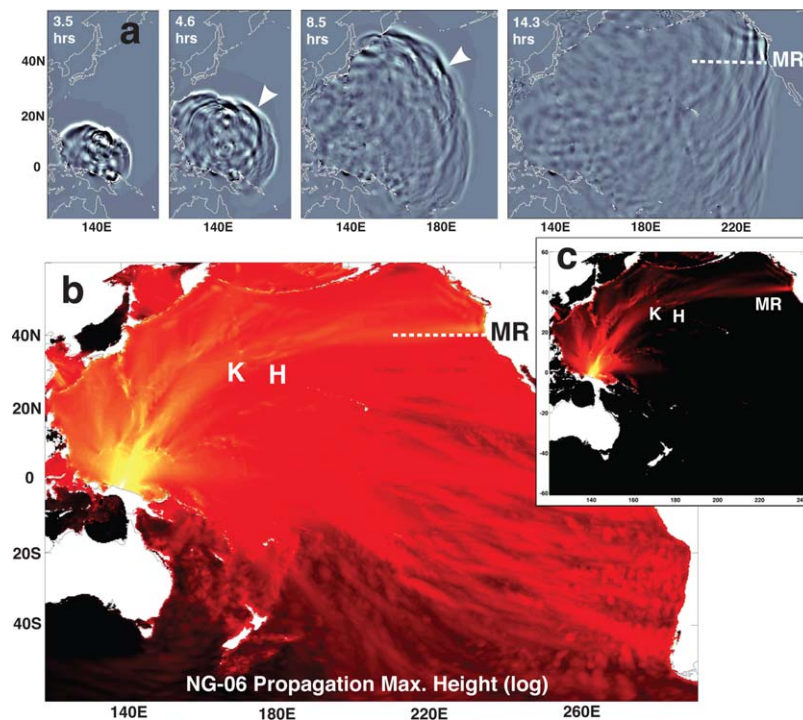
Figure 6. Tsunami propagation from central New Guinea (source NG-006). (a) Time series showing early development of constructive interference patterns that reach the North American coast. (b) Maximum wave height across Pacific. (c) Maximum wave height with color range mapped to enhance visibility of larger waves. The amplitude range mapped on the inset has been narrowed and shifted upward to show more detail in the highest energy pathways. Mendocino Ridge (MR) indicated with dotted line, K = Koko Guyot, H = Hess Ridge.

Figure 7. (a) Bathymetry crossing the Mendocino Ridge along meridian 210°E (black) at western end, and 233°E (red) at eastern end. Tsunami amplitude before and afte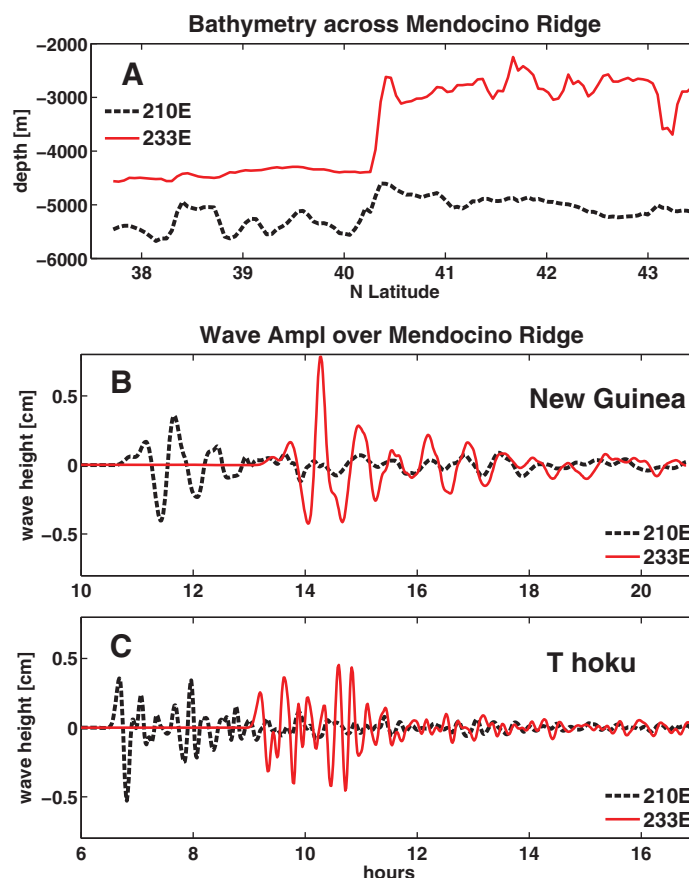r propagation over the ridge from (b) New Guinea source NG-006 and (c) Tōhoku/Japan source KI-026. Black line is tsunami amplitude before crossing the ridge (210°E) and red line is near the end of transit over the ridge (233°E). Both are amplitudes just north of the ridge crest at 41.6°N.

To view the development of this high-energy branch, we can look at the propagation time series of wave height (Figure 6a). At 3.5 h there is already significant disturbance of the tsunami from the many small islands and submerged seamounts. The center of the leading wave is beginning to pass over the rows of trenches and ridges on the east side of the Philippine Sea. At 4.6 h this section of the wavefront has slowed and the segment to its west is advancing past it (the white arrow tracks this segment). There are distinct regions of higher and lower wave energy developing from the interference patterns, with peak amplitudes on these two segments. At 8.5 h the leading edge is approaching the Aleutians and the two high-energy segments are still visible, one passing directly over Koko Guyot. As the tsunami continues across the North Pacific, the northern segment crosses into the Bering Sea and the other proceeds directly over the Mendocino Escarpment, where additional focusing occurs closer to the Crescent City target. *Barberopoulou et al.* [2014] describe similar processes of topographic scattering and focusing by refraction along ridges that likely influenced the distribution of energy from the 2011 Tohoku tsunami on the U.S. West Coast, in particular the "prefocusing" that can occur when westward-propagating waves encounter the Koko Guyot/Hess Ridge system en route to the Mendocino Ridge.

Waves propagating from the SW Pacific maximum-amplitude source for Los Angeles (MO-05, 2.7°S, 151.8°E, near the Solomon Islands) have similar elevated amplitudes near the source, but one high-energy branch passes over the Hawaiian Island/Emperor Seamount chain, causing strong secondary waves that superimpose and are deflected toward Southern California. Along this more southerly path, there is no further disturbance or amplification from bathymetry as the wave propagates toward the Southern California Bight.

4.2. Northeast Pacific: Amplification by Mendocino Ridge

Across the eastern portion of the Mendocino fracture zone, the seafloor is 1000 m deeper on the south compared to the north, and the narrow ridge crest (approximately 10–30 km wide) rises from approximately 3000 m to as little as 1100 m depth. Focusing of energy occurs both along and immediately north of the Mendocino Ridge (MR). Tsunami wave refraction along the ridge occurs due to decreasing water depth along the ridge crest. Additional focusing of wave energy develops due to the sharp depth difference between the north and south sides of the MR (Figure 7a, 233°E profile), which causes bending of the deeper, faster waves toward the MR from the south. North of the MR, the phase speed and wavelength of the leading wave is approximately 20% greater than south of the MR (Table 1).

Table 1. Tsunami Characteristics North and South of the Mendocino Ridge[a]

Location	Depth (m)	Phase Speed (km/h)	Wavelength (km)	Period (min)
233°E, 41.62°N	3287	643	431	40.2
233°E, 39.18°N	4042	768	515	40.2

[a]Model propagation from New Guinea unit source NG-06, 2.5°S, 139.6°E.

These differences across the MR result in perturbation of the tsunami wave propagation by differential refraction of wave energy directly over the narrow ridge crest, and also because of the broader refractive zone to the north of the crest due to the step-like depth change to either side. The refraction of the faster moving waves to the south causes bending and concentration of energy to the north, peaking at about 41.6°N.

The process of refractive amplification along Mendocino was described by *Kowalik et al.* [2008] for the November 2006 Kuril Islands tsunami, which approached Mendocino from the northwest. In that event, energy flux calculations showed that focusing was minimal from the primary wave, which was oriented almost parallel to the Mendocino ridge upon impact. But secondary source waves from interaction with Kinmei and Hess were amplified by almost a factor of 4, to the point that their amplitudes were larger than the original tsunami source. The area of amplification was over the same narrow band just north of the ridge (41°N–42°N).

To examine the effect of the Mendocino Ridge on focusing both primary and secondary tsunami arrivals, we compare the wave characteristics and spectra of an eastward-propagating tsunami before and after interaction with the ridge (similar to the comparison of background spectra and tsunami spectra by *Rabinovich* [1997]) to distinguish between the incoming tsunami source signal and locally induced disturbances). Each transect extends from approximately 37.5°N–43.5°N, with the preridge transect along the 210°E meridian, and the postridge transect just offshore of the California/Oregon shelf at the 233°E meridian (Figure 7a, bathymetric profiles). The tsunami origin is the New Guinea source (NG-06, 2.5°S, 139.6°E) that displays high amplification over a narrow band along the MR (Figures 6b and 6c). Just north of the ridge crest, the amplitude of the leading wave and successive crests can be seen to double as the wave progresses over the ridge between 210°E and 233°E (Figure 7b).
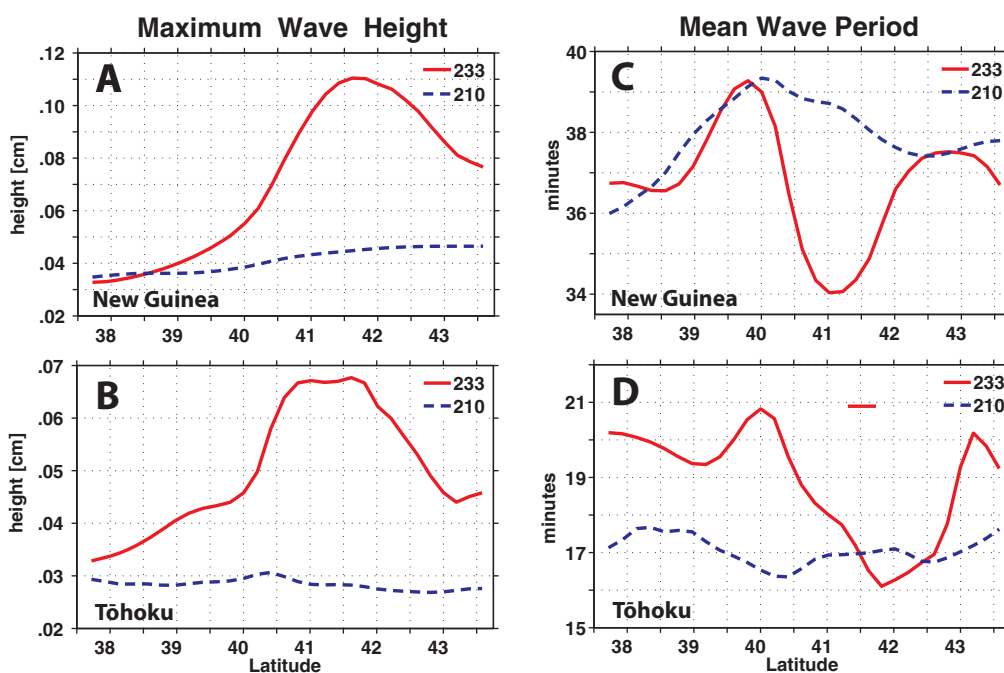

Figure 8. (a, b) Maximum wave height and (c, d) mean wave period of tsunami propagating over transects perpendicular to Mendocino Ridge at 210°E (red) and 233°E (blue) as a function of distance from the ridge crest. Figures 8a and 8c are from New Guinea source NG-06, Figures 8b and 8d are from Tōhoku/Japan source KI-26. Mendocino Ridge is at approximately 40.3°N.
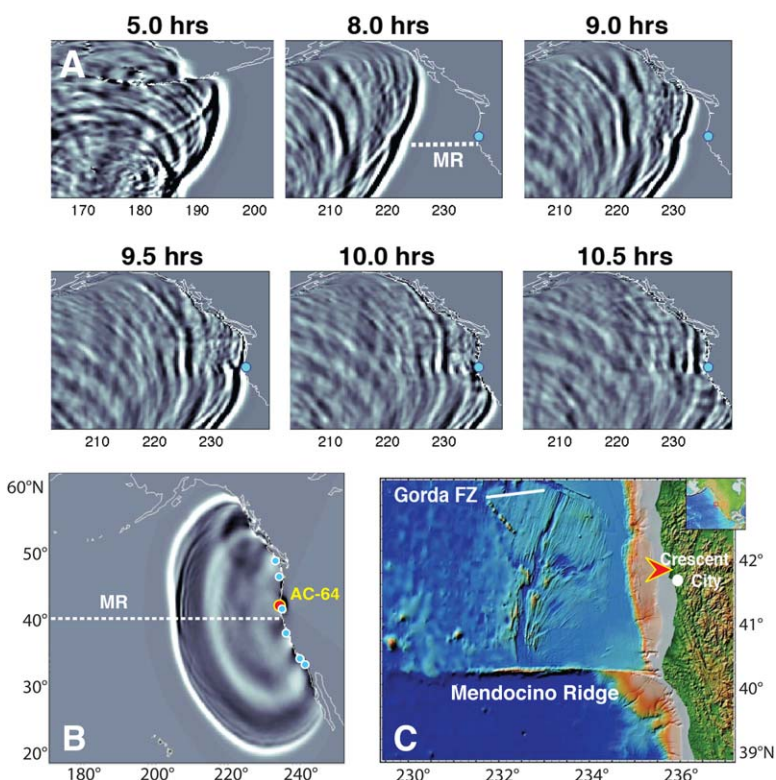
Figure 9. (a) Model tsunami propagation spatial patterns over the Mendocino Ridge (MR) from the Tōhoku Japan 2011 earthquake epicenter (unit source KI-026, 38.58°N, 142.76°E) at progressive times after generation (top six figures). The MR extends offshore from the coast at Cape Mendocino, about 160 km south of Crescent City (blue dot). (b) Spatial pattern from unit source AC-64 (red dot, 41.98°N, 235.96°E), south of Crescent City, CA, 3.5 h after initiation. Target locations are indicated with blue dots. (c) Topography of the region near MR (source AC-64 at red arrow).

The maximum wave amplitude occurs at 41.6°N, more than a degree north of ridge axis (Figure 8a). The mean wave period between 40.0° and 42.5°N also changes between the 210°E and 233°E ridge transects (Figure 8c). From 38 to 40° the wave period increases with proximity to the ridge axis at both 210°E and 233°E, from 36 to 39 min, as the depth (and therefore wave speed) decreases. North of the axis, wave period along the 210°E transect gradually decreases as the water depth slowly increases. However, at 233°E, where the depth remains shallow north of the ridge axis, the mean period decreases rapidly to a minimum of 34 min at 41.0°N–41.1°N before returning to a level closer to the 210°E transect north of 42°N. This is the latitude band where wave amplitude doubles on the 233°E transect. Clearly there are contributions from higher-frequency components that are not present before propagation over the ridge.

Tsunami propagation from the source near the epicenter of the 2011 Tōhoku/Japan earthquake is also affected by the Mendocino ridge (Figure 9a). At the 5 h mark after generation, the northern edge of the primary source pulse passes along the Aleutian Islands, while farther south, interaction with the Kinsei Seamount and Hess Ridge (just above the 180° longitude marking) slows the leading wave front's advance. These topographic features initiate secondary waves, which encircle the area. At 8 h, the primary wave is starting to travel down the North American coast, and the secondary wave lags at about 210°E. Approaching the coast at 9–9.5 h, the primary wavefront is refracted somewhat along the ridge axis, but it is the secondary wave (now at 220–225°E) that is amplified on the north side of the Mendocino Ridge, while wave height to the south diminishes along a sharp boundary (9.5–10.5 h).

Similar to the New Guinea source, the tsunami propagating from Tōhoku also exhibits increased wave height after transiting the Mendocino Ridge (Figure 7c), but with some notable differences. On approach to the ridge (black dotted line) the shorter period Tōhoku wave appears to have more high-frequency, secondary components from interference earlier on its path. The initial wave height is similar to the New Guinea wave, but the amplitude after propagation over the ridge (solid red line) is significantly lower, and the highest crest lags the wave arrival by 2 h. While the maximum wave height also occurs north of the ridge crest

at 41.6°N, it is nearly 40% lower (Figure 8b) and the amplification on either side of the ridge crest is distributed more irregularly. The difference in response to bathymetry is consistent with the difference in mean wave period, which exhibits the largest contrast between the two tsunami sources (Figure 8d). Both have the longest period waves near the ridge crest, and the shortest period waves 1–2° north of the crest. But, notably, the mean wave period of the Tōhoku source is shorter than the SW Pacific source by half overall, again suggesting prior interference, scattering, or influence of secondary sources.

Spectra of the waves propagating across the two transects exhibit significant differences in both magnitude and frequency of the spectral peaks from the ridge crest (40.3°N) northward. Both transects have maximum energy peaks at 4–5×10^{-4} Hz (approximately 37 min period) (Figures 10a and 10b). South of the ridge crest, the energy levels at this frequency are similar in both transects. However, north of the ridge crest, the energy at the 233°E stations increases up to 10 dB compared with the 210° locations, with maximum energy levels near 41.7°N. Additional energy peaks north of the ridge crest occur between 7×10^{-4} and 2×10^{-3} Hz south of 41.7°N. At 9×10^{-4} Hz (18 min period) the 10 dB peak between 40.5°N and 41.7°N is also accompanied by a 10 dB decrease between 42°N and 43°N. Long period energy at frequencies $<2 \times 10^{-4}$ Hz north of the ridge crest also displays slightly reduced energy levels at 233°E relative to 210°E. The spectral ratio of 233°/210° shows that the ridge crest (Figure 10c, solid black line) marks the point where the two transects' wave characteristics diverge. The largest energy difference is not at the peak frequency however, but at frequencies just higher and lower, indicating a broadening of the peak tsunami spectral band as well as an increase in amplitude.

Consistent with the shorter period and more disorganized signal from the Tōhoku source, shorter frequencies are also more dominant in its wave spectra (Figures 10e and 10f), with peak energy just above 10^{-3} Hz. After propagation along the ridge, spectral ratios reveal an energy increase in almost all frequencies between 10^{-4} and 10^{-3} Hz, with the greatest occurring immediately north of the ridge (40.5°N–41°N) centered on the 6–7×10^{-4} Hz band (approximately 25 min period), and between 41.5°N and 42°N near 10^{-3} Hz (15 min period) (Figure 10g).

Compared to the original tsunami signals, waves from both New Guinea and Japan have experienced a loss of high-frequency energy before arrival at the western boundary of the Mendocino Ridge, visible in the ratios of the 210°E spectra and the spectra close to each tsunami source (Figures 10d and 10h; near-source spectra are calculated from transects of the same length as those across the MR, oriented orthogonal to the source wave propagation direction). Reduction in higher-frequency spectral levels is consistent with scattering from small islands and bathymetric features in the West Pacific. By the time the wave from New Guinea source NG-006 arrives at the MR there has been an especially sharp drop of 50–75 dB at frequencies $>2 \times 10^{-3}$ Hz (periods <8 min), while lower frequencies show only small declines. By contrast, the Tōhoku wave path is shorter and travels over bathymetry with a somewhat lower scattering potential than the more bathymetrically complex SW Pacific. Here there is a small loss of energy at low frequencies and a mix of energy loss and amplification at midfrequencies. Energy loss at high frequencies is largest, but in comparison to NG-006 only drops by 20–30 dB.

4.3. Cascadia and Alaska: Low-Scattering Regions

In contrast to topographic effects on western Pacific sources, tsunami sources along the Pacific Northwest and Alaskan coasts encounter virtually no topographic obstacles, and interference is absent until source waves reflect off an adjacent coastline. Cascadian and Alaskan sources can result in large wave heights along the U.S. West Coast north of the Southern California Bight, but there is little irregularity in amplification among target sites, as seen in the wave pattern resulting from the south Cascadia source (AC-64, 41.98°N, 235.96°E) near Crescent City, CA (Figure 9b). From Alaskan sources, tsunami wavefronts approach nearly parallel to the Mendocino Ridge, minimizing the refractive focusing that occurs. Wavefronts from Cascadian sources would propagate nearly perpendicular to the ridge axis, but refraction effects appear to be minimal during the transit over shallow continental shelf waters. Encountering no reflective coastlines or scattering bathymetry as the wavefronts move westward, Cascadian sources produce the least disrupted propagation patterns along the Pacific Rim.

In their analysis of remote sources affecting Los Angeles and Long Beach harbors, *Uslu et al.* [2010] found Alaskan sources to be much stronger than they appear in open ocean propagation simulations, with magnitudes at Los Angeles similar to the high-amplitude sources in the Solomon Islands, but lower than high-
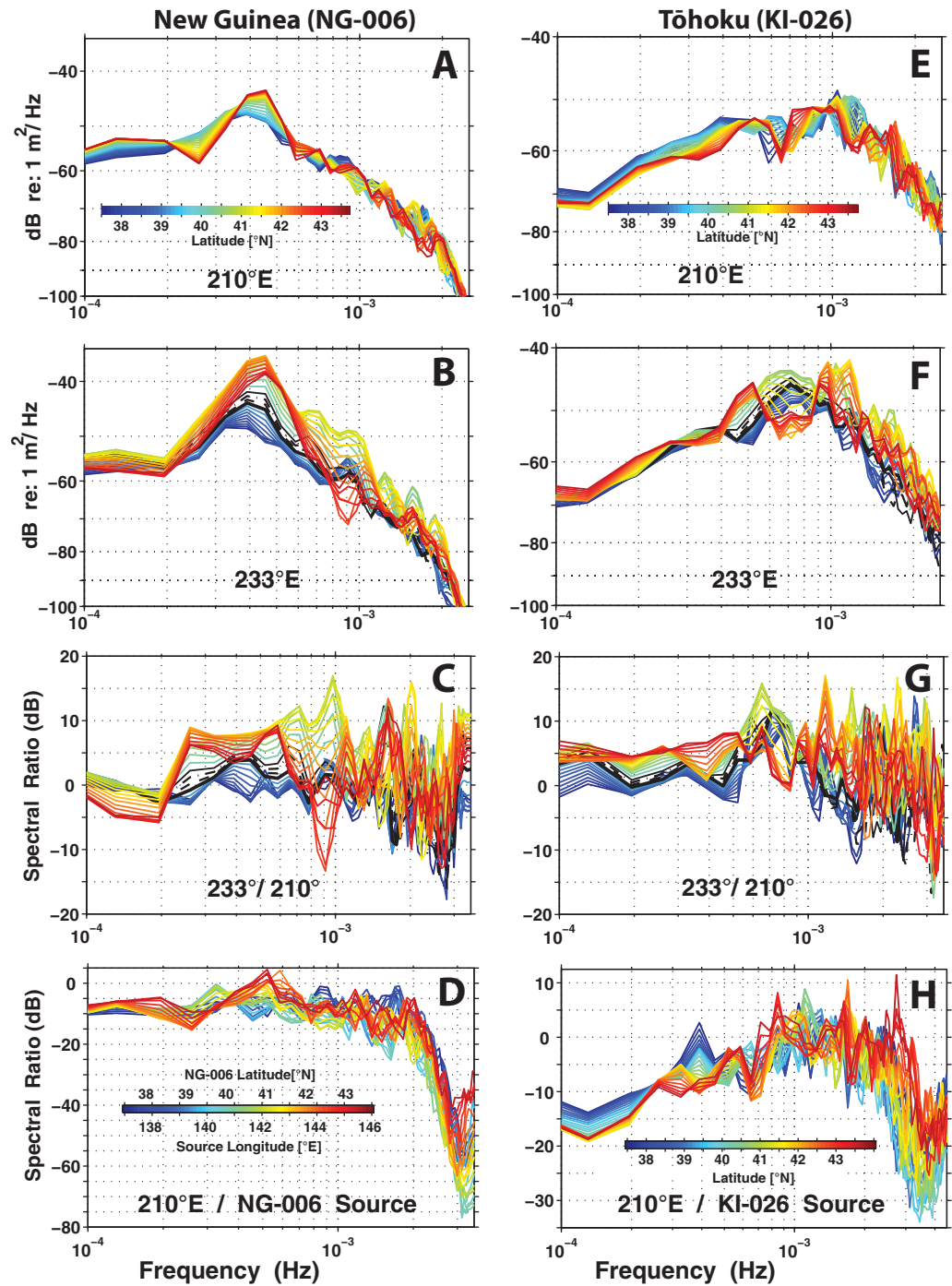
Figure 10. Wave spectra for tsunami propagating over transects located at the 210°E meridian (western extension of Mendocino Ridge) and the 233°E meridian (near the continental shelf at eastern extent of Mendocino Ridge) from sources in New Guinea (NG-006) and Tohoku Japan (KI-026). Color of spectral lines corresponds to transect position north or south of the ridge crest (blue at south, red at north). Black lines indicate the crest region. (a) New Guinea source wave crossing 210°E and (c) crossing 233°E. (c) Ratio of wave spectra from A and B (233°/210°). (d) Ratio of spectra crossing 210°E and spectra near the NG-006 source. (e) Tōhoku/Japan source wave crossing 210°E, and (f) crossing 233°E. (g) Ratio of spectra in Figures 10d and 10e (233°/210°). (h) Ratio of spectra at 210°E and spectra near the KI-026 source. Near-source spectra are calculated from transects of the same length as those across the MR, oriented orthogonal to the source wave propagation direction.

amplitude sources in Chile. Target location and model resolution may explain these differences, and the combined effect of using 20 unit sources by *Uslu et al.* [2010] may result in a strong cumulative effect not present when examining sources individually. Los Angeles Harbor has a south-facing exposure similar to

the Santa Monica region target, but its embayment is smaller and possibly less protected. The complex bathymetry within the Channel Islands region scatters wave energy through small-scale refraction, reflection, and diffraction, and may result in focusing tsunamis at particular locations along the coast not resolved in the open ocean propagation model. The *Uslu et al.* [2010] results are based on the fully nested NOAA model in which the unit source propagation simulation provides the input for a higher-resolution regional grid, whose output in turn provides the wavefield for a small-scale inundation model of the LA/Long Beach Harbor area. This allows for both better resolution of island interference, and the propagation of waves into nearshore areas that the open-ocean model does not include.

5. Discussion

The geographical locations of earthquake sources with high potential for damaging tsunamis on the U.S. west coast follow a similar pattern for key ports from Washington to southern California, but there are notable peaks in incoming wave energy specific to certain source-target combinations. Scattering, reflection, and refraction from complex bathymetry and the subsequent interference introduced by these secondary sources can cause wave energy from the original tsunami to become strongly concentrated in narrow high-energy pathways. In some cases bathymetry nearer the target may provide additional focusing. The result is relatively small stretches of coastline being impacted by anomalously high-amplitude waves. The most prominent example in this study occurs between New Guinea and Crescent City, where a narrow band of a secondary wave is amplified and subsequently undergoes refractive focusing along the Mendocino Ridge. Waves from sources at the Manus Trench and the Solomon Islands are similarly affected by remote bathymetry during propagation to Los Angeles and San Francisco, respectively. Presumably, due to the relatively narrow width of the high-energy branches that develop, and the way the branches shift in direction, many more source-target enhancement pairings such as this may exist.

5.1. Comparison With Historical Tsunamis

To understand the importance of source location on the potential for damaging tsunamis, the maximum-amplitude source locations identified with the NCTR propagation model are investigated in the context of extreme historical events. For instance, did the Chile 1960 earthquake occur at or near a maximum-amplitude source location, or could the resulting tsunami have been much worse if the epicenter was in a slightly different location? The largest tsunami-generating earthquakes in the Pacific have originated in three different regions: (i) South America/Chile 1960 (unit sources CS 93–95, Mw 9.5), (ii) North Pacific/Alaska 1964 (unit sources AC 37, 38, 238, Mw 9.2), and (iii) West Pacific/Japan 2011 (unit sources KI 26–27, Mw 9.0) (Figure 5, starred locations). To compare potential impacts from tsunamis hitting the West Coast, these historical events can be used to configure theoretical events at the maximum-amplitude source locations in each region. Using geological and seismic data, each historical tsunami has been simulated by NCTR with linear combinations of unit sources. The source configuration includes the number and arrangement of unit sources, and the slip distance multipliers for each source adjusted to equal the displacement magnitude of the historical event. For the theoretical comparisons, the configuration of unit sources in each historical event is replicated as nearly as possible with sources placed near each target's maximum-amplitude location in that region. For example, the configuration of the 1960 Chilean tsunami generated from unit sources CS 93–95 is used to generate a model tsunami from sources 108–110 (the maximum-amplitude source area for Juan de Fuca, Astoria, and Crescent City) and from sources CS 107–109, 87–89, and 90–92, the maximum-amplitude source areas for San Francisco, Los Angeles, and San Diego, respectively. This provides a comparable event for each of the targets at their most critical source location for generating a high-impact tsunami.

The wave height at each target location from the historical event (Table 2, event height) is compared with the wave height generated by the similarly configured event occurring at the maximum-amplitude location (Table 2, max source height). The difference between the two (Table 2, ΔH) provides a measure of what a "worst-case scenario" tsunami might produce in each region. A nondimensional amplification factor (max source height divided by historical event height) is given for each case to compare the relative impact between target locations.

The largest absolute increase in wave height produced by a Chilean-1960 magnitude tsunami is from 3.32 to 7.74 m (ΔH +4.42 m), which occurs at Los Angeles if the source area is shifted to CS 87–89 (about 600 km northward), giving an amplification factor of 2.3 greater than the 1960 event.

Table 2. Tsunami Height Comparison: Maximum Sources Versus Historical Events in Three Regions[a]

Target	Max Source Location	Max Source Height (m)	Hist. Event Height (m)	ΔH (m)	Amplif. Factor
A. South America: Chile 1960 Mw 9.5					
JDF	CS 108–110	1.24	0.81	0.43	1.6
ASA	CS 108–110	1.69	1.11	0.58	1.5
CCY	CS 108–110	1.95	1.12	0.83	1.7
SFO	CS 107–109	3.39	1.72	1.67	2.0
LAS	CS 87–89	7.74	3.32	4.42	2.3
SDO	CS 90–92	1.68	1.31	0.37	1.3
B. North Pacific: Alaska 1964 Mw 9.2					
JDF	AC 30–32	1.61	1.25	0.35	1.3
ASA	AC 30–32	2.24	1.57	0.67	1.4
CCY	AC 31–33	2.75	2.06	0.69	1.3
SFO	AC 30–32	3.44	2.52	0.92	1.4
LAS	AC 31–33	0.96	0.55	0.40	1.7
SDO	AC 32–34	1.13	0.61	0.52	1.9
C. West Pacific: Japan 2011 Mw 8.9					
JDF					
ASA	MO 01–03	0.62	0.26	0.36	2.4
CCY	NG 06–08	1.54	0.63	0.90	2.4
SFO	NV 09–11	0.72	0.49	0.23	1.5
LAS	MO 03–05	0.77	0.22	0.55	3.5
SDO					

[a]Unit sources associated with historical events are as follows: A. Chile 1960: CS 93–95; B. Alaska 1964: AC 37, 38, 238; and C. Japan 2011: KI 26–27.

For tsunamis originating in Alaska, sources 300–800 km southwest west of the 1964 epicenter generate the largest amplitude offshore waves at the U.S. target locations. The absolute wave height increase relative to the 1964 event is largest offshore San Francisco, from 2.52 to 3.44 m (ΔH +0.92 m, corresponding to an amplification factor of 1.4). However, the largest relative amplification factor is 1.9, off the coast of San Diego, although the wave height only reaches 1.13 m.

Tsunamis arriving at study targets on the U.S. West Coast from West Pacific sources have lower amplitude than from other regions. The West Pacific sources produce the highest absolute wave height (1.54 m) at Crescent City, with all others less than 1 m. Importantly, Los Angeles has the highest amplification factor, 3.5, the highest of any source-target combination overall. The locations of maximum-amplitude wave generation also display the greatest source-target specificity and influence of remote bathymetric scattering and focusing (e.g., New Guinea-Crescent City, Manus-Los Angeles). In contrast, there are no particular West Pacific sources that generate substantially stronger incoming tsunamis at the Juan de Fuca/Seattle and San Diego targets.

Not all tsunamigenic sources on the Pacific Rim are considered high risk for large earthquakes in the next 50–100 years, so high potential impact from a tsunami is not necessarily coupled with high hazard potential for an actual event. Along portions of some faults, such as the Aleutian-Alaskan megathrust, movement can occur without accumulation of strain, a process known as "aseismic slip." At the end of the Alaskan Peninsula, the Shumagin Gap (unit sources AC 26–28) is one such aseismic area where extreme earthquakes are assumed to be very unlikely, while the east end of the megathrust under Prince William sound is considered 0% aseismic [*Wesson et al.*, 2007]. Past large earthquakes releasing strain and geologic evidence suggesting low earthquake frequency may also put a region at low risk. The Alaskan 1964 earthquake ruptured from the epicenter at the far northeast of the megathrust under Prince William Sound all the way south along Kodiak Island, and the frequency estimate for PWS is about 650 years. However, the slip along Kodiak in 1964 was very small, estimated at only 0–5.5 m on all but the northernmost segment (AC-34) [*Johnson et al.*, 1996; *Mavroeidis et al.*, 2008]. While seismic hazard is not considered as high as in southeast Alaska (on the relatively nontsunamigenic Queen Charlotte strike-slip fault) [*Wesson et al.*, 2007] the potentially high-amplitude sources modeled just offshore and to the south of Kodiak are in an active area that had little or no slip in 1964 and are north of the aseismic Shumagin Gap. In South America, seismic risk is highest north of Santiago for approximately 600 km along the Peru-Chile trench, but also has an elevated region to the south that includes the Los Angeles and San Diego high-amplitude sources [*Petersen et al.*, 2010]. The four northern targets would only see a small absolute wave height from their maximum source regions in far southern Chile (CS 107–110) and it is not a high probability location for large earthquakes. Over much of the small island areas in the Western Pacific seismic risk is poorly characterized. However, all four of the maximum sources modeled are along the islands of New Guinea and Papua New Guinea, an area with plate movements of >10 cm/yr where the seismic hazard is considered a very high [*McCue*, 1999].

It should be noted that wave heights reported here as comparisons with historical events are the incoming, offshore heights at 500 m depth, not the amplitude at the shoreline. Consequently, they do not include the effects of traversing the continental shelf, nearshore bathymetric amplification, local shoreline configuration

(exposure), harbor geometry, or inundation potential. Accounting for these factors requires employing nested high-resolution coastal inundation models.

5.2. Source Region Effects on West Coast Tsunami Characteristics

Focusing of wave energy over the Mendocino Ridge (MR) is the primary topographic interaction that can increase tsunami amplitude once they are in transit over the NE Pacific. However, tsunamis originating in the NW and SW Pacific exhibit different responses that appear to be related to the intervening bathymetry rather than the direction of approach. Spectra from the NW Pacific (Tōhoku Japan) contain more high-frequency energy at the outset, before interacting with the ridge, with peak energy for waves with periods around 15 min (approximately 10^{-3} Hz) (Figure 10e). As with the SW Pacific source, waves to the north of the ridge crest undergo a large increase in energy while propagating over the MR, with the largest amplitude increase occurring around 41.6°N. In contrast to the SW source however, the energy peak near the ridge occurs at a lower frequency (25 min period). The Tōhoku wave also displays evidence of significant pre-MR scattering and contributions from secondary sources. Remote bathymetry focuses tsunami energy from the New Guinea source before its arrival at the MR, which is subsequently amplified further during propagation over the ridge. In contrast, remote bathymetric effects have scattered and reduced energy from the Tōhoku source prior to arrival at the ridge. While the less complex waveform of the New Guinea source produces a larger leading wave near the ridge, the higher frequencies in the Tōhoku wave result in a series of closely spaced amplified crests arriving in quick succession, with the maximum amplitude occurring 2 h after the initial crest. Bathymetric interactions such as these that alter wave spectral distributions are potentially an important factor in determining the ultimate wave heights approaching the coast, as well as their timing.

In addition to focusing by relatively small-scale seafloor features, much larger-scale bathymetry can have a similar effect. Ray tracing studies of tsunami wave propagation across the Pacific that require smoothing the bathymetry eliminate or greatly diminish many of the features responsible for scattering and interference, especially islands and seafloor ridges [e.g., *Satake*, 1988]. While bathymetric smoothing is viewed as a limitation in ray tracing, it is nevertheless a useful model to distinguish the influence of small-scale bathymetry versus large-scale depth contours on wave amplitude enhancement. Of the four Pacific Rim locations that *Satake* [1988] modeled (southern Chile, the Aleutians, Japan, and the Solomon Islands), the strongest focusing was observed between the Solomon Islands source (5°S, 154°E) and northern California, the same West Coast region that exhibits amplification by refraction from the Mendocino Ridge in the NCTR propagation model. This result implies that tsunamis from the SW Pacific are affected at the outset by nearby large-scale bathymetric contours, and then may experience further focusing while traversing the Pacific and approaching the coast of North America. By contrast, ray tracing of sources in the Aleutians and Japan does not exhibit the focusing toward North America that is seen in the NCTR results, suggesting that interaction with small-scale mid-Pacific features (e.g., seamounts and guyots in the Hawaiian-Emperor chain) may be responsible for most or all of the focusing of wave energy traversing those areas, followed by subsequent interaction with the Mendocino Ridge. The variety of scales involved in wave amplification by remote focusing is an important consideration in the selection of bathymetry for tsunami modeling.

6. Conclusions

The U.S. West Coast is vulnerable to arrivals of strong tsunami events. However, only a few earthquake locations around the Pacific Rim have historically generated tsunamis that have produced significant impacts along this coast. In order to better understand coastal vulnerability, we examined the output of numerous tsunami model simulations of wave patterns excited by earthquakes around the Pacific Rim. These hazards were organized by distance from source and direction of source to further illuminate their characteristics. In order to analyze the characteristics of the tsunami paths that may be responsible for their high energy, we identified the source locations of model tsunamis that arrive with highest amplitude at key U.S. West Coast port locations, including major population centers in California, Oregon, and Washington.

While each port is vulnerable to local earthquakes generating tsunamis, several remote locations are often equally effective at producing high-amplitude waves along the West Coast. For example, model tsunamis from Alaskan earthquakes have a high amplitude relative to other sources at all studied port locations when the source is within 500 km of Kodiak Island. Distant trans-Pacific locations, such as sections along

New Guinea, the Solomon Islands, and Yap, can also generate tsunamis that threaten specific regions of the U.S. West Coast.

These revealed key topographic controls on the focusing of wave energy by distant scattering and interference from southwest Pacific islands and seamounts near tsunami sources, Hess Ridge and Koko Guyot in the central Pacific, and the Mendocino Ridge on approach to the U.S. West Coast. These features alter tsunami spectral characteristics, affecting the impact of subsequent bathymetric interactions as well as the timing and magnitude of the waves that eventually reach shore. The source region generating these narrow, high-energy paths was often very small, as little as 100 km along a subduction zone, creating distinct source-target pairs that result in sharply amplified wave energy local to that target. It is likely that similar high-amplitude source-target pairings exist for other coastal targets which would result in disproportionately large impact should a large seismic event occur.

The source characteristics and model wave propagation of the three largest Pacific earthquakes that generated large tsunami in 1960 (South America/Chile), 1964 (NE Pacific/Alaska), and 2011 (W Pacific/Japan) were used to model comparable events occurring at the highest amplitude sources in each of these regions for each key port. These showed that the historical locations did not coincide with the maximum source locations, and as a result tsunamis generated in these locations could be larger by a factor of 1.3–3.5 (30–350%).

The model simulations of tsunamis provide an extensive view of the most hazardous locations for earthquakes generating events that could significantly impact the U.S. West Coast for large earthquakes that efficiently couple ocean bottom displacements into the barotropic component of the oceanic flows. Other effects that were not included in this study could significantly change the local response, including topographic channeling by smaller-scale features not resolved in the model, nonlinear effects of large-amplitude wave propagation, shoaling and breaking, and local resonance due to coastal morphology.

References

Arcas, D., and H. Segur (2012), Seismically generated tsunamis, *Philos. Trans. R. Soc. A*, *370*, 1505–1542, doi:10.1098/rsta.2011.0457.

Arcas, D., and B. Uslu (2010), A Tsunami Forecast Model for Crescent City, California, in *NOAA OAR Special Report*, *PMEL Tsunami Forecast Ser.*, vol. 2, 112 pp., NOAA/Pacific Marine Environmental Laboratory, Seattle, Wash.

Barberopoulou, A., M. R. Legg, E. Gica, and G. Legg (2014), Multiple wave arrivals contribute to damage and tsunami duration on the US West Coast, in *Tsunami Events and Lessons Learned, Adv. Nat. Technol. Hazards Res.*, vol. 35, edited by Y. A. Kontar, V. Santiago-Fandiño, and T. Takahashi, pp. 359–376, Springer, Dordrecht, Netherlands.

Fuller, J. D., and L. A. Mysak (1977), Edge waves in the presence of an irregular coastline, *J. Phys. Oceanogr.*, *7*(6), 846–855.

Gica, E., M. Spillane, V. V. Titov, C. Chamberlin, and J. C. Newman (2008), Development of the forecast propagation database for NOAA's short-term inundation forecast for tsunamis (SIFT), in *NOAA Tech. Memo. OAR PMEL-139*, 89 pp, NOAA/Pacific Marine Environmental Laboratory, Seattle, Wash.

Gonzalez, F. I., K. Satake, E. F. Boss, and H. O. Mofjeld (1995), Edge wave and non-trapped modes of the 25 April 1992 Cape Mendocino tsunami, *Pure Appl. Geophys.*, *144*, 409–426.

Holmes-Dean, L., M. Hendershott, P. D. Bromirski, and R. E. Flick (2015), Spectral characteristics of the 1960 tsunami at Crescent City, CA, *Sci. Tsunami Hazards*, *34*(2), 67–82.

Horrillo, J., W. Knight, and Z. Kowalik (2008), The Kuril Islands tsunami of November 2006: 2. Impact at Crescent City by local enhancement, *J. Geophys. Res.*, *113*, C01021, doi:10.1029/2007JC004404.

Johnson, J. M., K. Satake, S. R. Holdahl, and J. Sauber (1996), The 1964 Prince William Sound earthquake: Joint inversion of tsunami and geodetic data, *J. Geophys. Res.*, *101*, 523–532, doi:10.1029/95JB02806.

Keulegan, G. H., J. Harrison, and M. J. Mathews (1969), Theoretics in design of the proposed Crescent City harbor tsunami model, *Tech. Rep. H-69-9*, 124 pp., U.S. Army Corps of Eng., Waterw. Exp. Stat., Vicksburg, Mass.

Kowalik, Z. (2008), Energy flux as a tool in locating tsunami secondary sources, *Sci. Tsunami Hazards*, *27*(3), 1–29.

Kowalik, Z., J. Horrillo, W. Knight, and T. Logan (2008), The Kuril Islands tsunami of November 2006: 1. Impact at Crescent City by distant scattering, *J. Geophys. Res.*, *113*, C01021, doi:10.1029/2007JC004402.

Mavroeidis, G. P., B. Zhang, G. Dong, A. S. Papageorgiou, U. Dutta, and N. N. Biswas (2008), Estimation of strong ground motion from the Great 1964 Mw 9.2 Prince William Sound, Alaska, *Earthquake Bull. Seismol. Soc. Am.*, *98*, 2303–2324, doi:10.1785/0120070273.

McCue, K. F. (1999), Seismic hazard mapping in Australia, the Southwest Pacific and Southeast Asia, *Ann. Geof.*, *42*(6), 1191–1198.

Mofjeld, H. O., V. V. Titov, F. I. Gonzalez, and J. C. Newman (2000), Analytic theory of tsunami wave scattering in the open ocean with application to the North Pacific, *NOAA Tech. Memo. OAR PMEL-116*, 38 pp., PMEL, Seattle, Wash.

Mofjeld, H. O., V. Titov, F. Gonzalez, and J. Newman (2001), Tsunami scattering provinces in the Pacific Ocean, *Geophys. Res. Lett.*, *28*, 335–338, doi:10.1029/2000GL011710.

Munk, W., F. Snodgrass, and G. Carrier (1956), Edge waves on the continental shelf, *Science*, *123*(3187), 127–132.

Murty, T. S. (1977), *Seismic Sea Waves: Tsunami*, 377 pp., Dep. of Fish. and the Environ. Fish. and Mar. Serv., Canada.

Mysak, L. A. (1980), Topographically trapped waves, *Ann. Rev. Fluid Mech.*, *12*(1), 45–76.

Petersen, M., S. Harmsen, K. Haller, C. Mueller, N. Luco, G. Hayes, J. Dewey, and K. Rukstales (2010), Preliminary seismic hazard model for South America, *Proceedings of Conferencia Internacional en Homenaje a Alberto Giesecke*, CERESIS, Lima, Peru.

Rabinovich, A. (1997), Spectral analysis of tsunami waves: Separation of source and topography effects, *J. Geophys. Res.*, *102*, 12,663–12,676, doi:10.1029/97JC00479.

Rabinovich, A. B., R. E. Thomson, and F. E. Stephenson (2006), The Sumatra tsunami of 26 December 2004 as observed in the North Pacific and North Atlantic oceans, *Surv. Geophys.*, *27*(6), 647–677, doi:10.1007/s10712-006-9000-9.

Roberts, J., and E. K. Kauper (1964), The effects of wind and precipitation on the modification of South Beach, Crescent City, California. Including an appendix on the focusing of tsunami energy at Crescent City, prepared by C.-W. Chien, *Final Rep., Contrib. DA-49-092-ARO-38*, 98 pp., Environ. Sci. Div., Dep. of the Army, Washington, D. C.

Satake, K. (1988), Effects of bathymetry on tsunami propagation: Application of Ray tracing to tsunamis, *Pure Appl. Geophys.*, *126*, 27–36.

Tang, L., V. V. Titov, and C. D. Chamberlin (2010), A Tsunami Forecast Model for Hilo, Hawaii, *NOAA OAR Special Report*, *PMEL Tsunami Forecast Ser.*, vol. 1, 94 pp, NOAA/Pacific Marine Environmental Laboratory, Seattle, Wash.

Titov, V., and F. I. González (1997), Implementation and testing of the method of splitting tsunami (MOST) model, *NOAA Tech. Memo. ERL PMEL-112 (PB98–122773)*, 11 pp., NOAA/Pacific Mar. Environ. Lab., Seattle, Wash.

Uslu, B., M. Eble, V. V. Titov, and E. N. Bernard (2010), Distant tsunami threats to the ports of Los Angeles and Long Beach, California, *NOAA OAR Special Report*, *Tsunami Hazard Assess. Spec. Ser.*, vol. 2, 100 pp., NOAA/Pacific Marine Environmental Laboratory, Seattle, Wash.

Wesson, R. L., O. S. Boyd, C. S. Mueller, C. G. Bufe, A. D. Frankel, and M. D. Petersen (2007), Revision of time-independent probabilistic seismic hazard maps for Alaska, *U.S. Geol. Surv. Open File Rep., 2007-1043*, 33 pp.